Upscaling of radionuclide transport and retention in crystalline rocks exhibiting micro-scale heterogeneity of the rock matrix

Paolo Trinchero[a], Vladimir Cvetkovic[b], Jan-Olof Selroos[c], Dirk Bosbach[d], Guido Deissmann[d]

[a]*AMPHOS 21 Consulting S.L., c/Veneçuela, 103, 08019 Barcelona, Spain*
[b]*KTH Royal Institute of Technology, Land and Water Resources Engineering, Teknikringen 76, 10044 Stockholm, Sweden.*
[c]*Swedish Nuclear Fuel and Waste Management Company, Box 3091, SE-169 03 Solna, Sweden*
[d]*Institute for Energy and Climate Research: Nuclear Waste Management and Reactor Safety (IEK-6) and JARA-HPC, Forschungszentrum Jülich GmbH, 52425 Jülich, Germany*

Abstract

In different in-situ diffusion experiments carried out in fractured crystalline rocks, sorbing radionuclides have shown a behaviour that strongly differs from what is predicted by homogeneous-based models. Their breakthrough curves are in fact often characterised by a fast first-arrival and these radionuclides can penetrate surprisingly long distances deep into the matrix. The heterogeneous structure of mineral distribution and porosity geometry had been offered as an explanation for these discrepancies. Here, we use reactive transport simulations to investigate the effect of the sparse distribution of sorption sites on the breakthrough curves of sorbing radionuclides. At small scale, the computed breakthrough curves significantly differ from those predicted using homogeneous models. For instance, the early part of these curves does not show any clear separation with the corresponding part of the curve of a non-sorbing tracer and a long transition zone is observed, with a very smooth slope of the tailing. Two different upscaling strategies, aimed at propagating the signal of heterogeneous retention over larger scales, are proposed and demonstrated against independent solutions computed at intermediate scales. The upscaling strategies are also used to show that at large scales (e.g. the scale of interest in a safety assessment study for a deep geological repository for nuclear waste) the signature of mineralogical heterogeneity is smoothed out and the heterogeneous breakthrough curve is well approximated by a homogeneous solution where the radionuclide distribution coefficient for the pure mineral phase is scaled by the mineral volume fraction. However, the spatial persistence of the heterogeneous signature is significant when the sorbing mineral is present in a low amount.

Keywords: mineralogical heterogeneity, heterogeneous retention, fractured media, upscaling

---

1. Introduction

Since the pioneering work of Fried et al. [1], considerable efforts have been devoted to understanding, characterising and modelling the retention capacity of the rock matrix for radionuclides. In fact, the capacity of the rock matrix to retain potentially harmful radionuclides is a *sine qua non* condition for the consideration of a crystalline rock system as a potential host for the geological disposal of spent nuclear fuel.

Different analytical solutions [e.g. 2, 3, 4] and mathematical formulations [e.g. 5, 6, 7] have been developed to account for the influence of matrix retention on radionuclide transport in fractured media, and particular emphasis has been placed on analysing the effects of matrix diffusion and sorption processes on the radionuclide breakthrough curves observed at a fracture outlet [8].

In all the studies mentioned above, radionuclide retention properties are assumed to be constant in the whole rock matrix. In parallel to the increasing availability and reliability of micro-characterisation methods, such as X-ray micro-computed tomography (X-µCT) or the ^{14}C-PolyMethylMethAcrylate (14C-PMMA) method [9, 10], recently efforts have been placed in understanding the influence of the heterogeneity of the matrix of crystalline rocks on radionuclide diffusion and retention. Sardini et al. [11] interpreted data of an out-diffusion experiment performed on a core sample of Palmottu granite (Eastern Finland) using time domain random walk simulations. The calculations were carried out in an inverse fashion on a two-dimensional porosity map obtained using the 14C-PMMA method. The results of this study point out that, at the investigated spatial scale, the considered granite behaves as a composite system, with micro-cracks acting as preferential diffusive pathways and with microporous zones controlling the late-time diffusive discharge. The composite behaviour of the rock matrix of crystalline rocks was also pointed out by other studies based on micro-characterisation data [e.g. 12, 13, 14]. At a larger scale, solutions that partly account for changes in diffusion and retention properties in the rock matrix were provided by Painter et al. [15], who used a time-domain Lagrangian framework to propose a piecewise approximation of changes in diffusion and retention properties, and Cvetkovic [16], who included a layer-based parameterisation of the matrix. More recently, Trinchero et al. [17] developed a numerical framework for the dynamic update of the retention properties of the rock matrix based on changes of the background geochemical conditions. However, the upscaling of the afore-mentioned micro-scale results to a larger scale remains a largely unresolved issue [12].

In parallel to the modelling efforts, different in-situ experiments have been carried out to investigate the rock rention capacity; e.g. the TRUE Block Experiment [18] and the Long Term Sorption Diffusion Experiment (LTDE-SD) [19] at the Äspö Hard Rock Laboratory (HRL) in Sweden, the Water Phase Diffusion Experiment (WPDE) [20] at Onkalo (Finland) and the Grimsel migration experiment [21] (Switzerland). In some, if not all, of these experiments, models based on the assumption of homogeneity of the rock matrix fail to describe field observations, particularly for sorbing radionuclides [e.g. 22]. The heterogeneous behaviour observed in some of these experiments (e.g. the very long penetration depth observed for strongly sorbing radionuclides) has been attributed, in part, to the heterogeneous and sparse distribution of sorption sites [e.g. 13].

In this work we use numerical simulations and two novel upscaling methodologies to gain insight into the effect that the heterogeneous distribution of active mineral grains of the rock matrix (i.e. mineral grains that have the potential to retain radionuclides) has on radionuclide breakthrough curves in dual porosity systems. The sparse distribution of mineral grains is simulated using Bernoulli distributions that honour the considered bulk mineral volume fraction.

2. Problem formulation and research questions

The classical models of retention of solutes in fractures build on the work of Carslaw and Jaeger [23] who considered heat transfer in slabs. The mathematical solution of Carslaw and Jaeger was then used by Neretnieks [2] to quantify the effect of retention in crystalline fractures by matrix diffusion and sorption; this was the basis for all subsequent conceptual models of tracer transport in fractures with retention [e.g. 4, 7]. In all these approaches the micro-structure and processes related to sorption are homogenised, in the sense that sorption reactions are expressed by a single equilibrium distribution coefficient (K_d), while mineralogical heterogeneity is neglected. These homogenised models are a practical necessity. Microscopic heterogeneity in the rock matrix of crystalline rocks is clearly present both as mineralogical and structural (in form of micro-fissures) heterogeneity, yet the issue of its effect on radionuclide transport and its possible upscaling to larger scales has not been systematically studied.

In this work, we address the implications of physical and mineralogical heterogeneity of the rock matrix on radionuclide transport and retention by considering three scales as illustrated in Figure 1: i) the laboratory scale, ii) the field-scale, and iii) the site-scale. Our main focus is first to better understand the potential effect of micro-scale reactions and heterogeneity on tracer transport through fractures in cristalline rocks, and then to explore upscaling/homogenisation strategies that can be used in applications. The three specific research questions we address in this work are:

1. What are the potential effects of micro-scale heterogeneity on reactive tracer transport through fractures in crystalline rocks?
2. How can we account for the physical and mineralogical heterogeneity of the rock matrix when modelling radionuclide transport in fractured media?
3. What are the most efficient and reliable upscaling/homogenisation strategies?

Thus, our work assesses radionuclide transport at different spatial scales and is organised as follows. In the next section we summarise evidence of micro-scale heterogeneity in the crystalline matrix. Next in section 4, we build a detailed process-based model of reactive tracer transport in a single fracture on the laboratory scale, using state-of-art simulation tools. In section 5 we present and evaluate alternative strategies for upscaling from the laboratory scale to the field scale, while in section 6 we consider upscaling to the site scale. Finally we draw main conclusions in section 8.

3. Evidence of mineralogical heterogeneity

A number of characterisation studies, carried out in the context of safety analyses of deep geological repositories for nuclear waste, points out that the rock matrix of fractured crystalline media is highly heterogeneous [e.g. 24, 25]. This heterogeneity is not only related to the pore space available for diffusion (which is typically a complex distribution of inter- and intra-granular pore space [11, 26, 27]) but is also associated with the sparse distribution of chemically active mineral grains; that is, mineral grains that interact with the dissolved solute species.

For instance, a mineral phase that is particularly important in this context is biotite, a phyllosilicate mineral within the mica group that contains iron in its reduced form. Biotite (and its alteration product chlorite) is in fact considered as an important buffer against the infiltration of oxidative redox fronts [28, 29, 30]. Moreover, biotite has a high sorption capacity and a high affinity with potentially harmful radionuclides, such as cesium [31].

Observations made with microscopy in a granitic rock sample taken at Forsmark (the site selected for geological disposal of high-level radioactive waste in Sweden) suggest that a typical biotite crystal has an average size of $\sim$ 400 x 200 µm^2 ($\sim$ 0.08 mm^2) although aggregates of grains up to 2 mm^2 can also be found [32]. A simple visual inspection of the pothomicrographs shows that biotite grains are indeed sparsely distributed (Figure 2).

Besides direct evidence, the existence of a heterogeneous and sparse distribution of sorption sites, and its relevance for the diffusion patterns of sorbing radionuclides, has also been inferred from the results of different in-situ experiments. One of these experiments is the Long Term Sorption Diffusion Experiment (LTDE-SD) carried out at the Äspö Hard Rock Laboratory (HRL) in Sweden. In the experiment, 21 radionuclide trace elements and one stable trace element were injected, circulated and sampled for around 200 days in a closed borehole section [33]. The trace elements included non-sorbing and sorbing tracers. Two borehole sections were put in contact with the tracer labelled groundwater: the first section was part of a natural fracture surface whereas the second section was in the unaltered matrix rock, devoid of natural fractures. One of the autoradiography analyses carried out on different core samples taken from the investigated rock volume is shown in Figure 3. Although no independent calibration was performed to separate the contributions from the different radionuclides, it is thought that the black areas of the autoradiography are generated mostly by cesium (namely, the isotope Cs-137), although other nuclides such as Ni-63 and Na-22 might also partly contribute to the blackening. These black areas correlate well with the distribution of areas with dark (mafic) minerals (e.g. biotite and chlorite, titanite and amphibole) (see the photography of the core in Figure 3), which points out the evident control of the sparse distribution of sorbing minerals on the diffusion of strongly sorbing radionuclides.

4. Cesium transport in a fracture with a physically and mineralogically heterogeneous matrix

The domain considered is a single fracture-matrix system of dimension 0.25 m x 0.1 m x $4.7{\cdot}10^{-3}$ m. The fracture is parallel to the x-z plane and has an half aperture of $2.5{\cdot}10^{-4}$ m. The domain was discretised with 7,600,000 regular grid cells of dimension δ=$2.5{\cdot}10^{-4}$ m (i.e. same size of the fracture half-aperture).

The heterogeneity of the matrix was simulated using a micro-DFN approach similar to that described in Svensson et al. [27]; i.e. three different fracture sets of length from one to a few millimeters were used to mimic grain-boundary pores as well as micro fractures that transect different mineral grains.

The micro-DFN was generated using the finite-volume groundwater flow simulator DarcyTools [34, 35]. In DarcyTools, fracture orientation follows a Fisher distribution (but here a random orientation was used) and spatial centers are statistically independent and follow a Poisson process. The generation of fractures is governed by the following equation:

$$n = \frac{I}{a}\left[\left(\frac{l+dl}{l_{ref}}-\right)^{a} - \left(\frac{l}{l_{ref}}\right)^{a}\right] \tag{1}$$

where n is the number of fractures per unit volume, I [1/m^3] is the intensity, a [-] is the power law exponent, l [m] is the fracture length and l_{ref} [m] is the reference length, which was here set to 1 m. The micro-DFN was constructed using the same fracture recipe used by Svensson et al. [27] to model a through-diffusion experiment carried out in a rock sample taken at Forsmark (Table 1). The micro-DFN was then represented onto the underlying continuum grid using the formulation provided by Svensson [36, 37], thus obtaining DFN-derived values of porosity and pore diffusivity (Figure 4).

The fracture water volumetric flux was set to 10^{-8} m/s and a first calculation was run where a non-sorbing tracer was injected along the inlet boundary of the fracture for a short period of time. This simulation and all the numerical calculations presented in this section were run on the supercomputer JUQUEEN of the Jülich Supercomputing Centre [38] using the reactive transport code PFLOTRAN [39, 40].

Snapshots of tracer concentration computed after 1 yr and 8 yr from the beginning of the injection are shown in Figure 5. The finger-shaped penetration profiles are related to preferential diffusive pathways, which in turn correspond to zones of the matrix with higher intensity of micro-fractures and grain boundary pores. The breakthrough curve computed at the fracture outlet was fitted with Sudicky's analytical solution [4] by setting the matrix porosity to the average value of the heterogeneous field ($\bar{\phi} = 2.2 \cdot 10^{-3}$) and using pore diffusivity as the only calibration parameter. The resulting fit, which was obtained with a value of pore diffusivity $D_p = 3.5 \cdot 10^{-13}$ m^2/s, is shown in Figure 6. The late-time deviation from the -3/2 slope of the breakthrough curve is due to the limited extension of the matrix. The generally good agreement between the heterogeneous model and the homogeneous-based analytical solution indicates that the behaviour of a non-sorbing tracer can be described using a homogeneous model parameterised based on equivalent parameters.

In the reactive transport calculations, a typical Littorina-type water (e.g. Trinchero et al. [30] and references therein) was used as resident water. The composition of the groundwater is listed in Table 2. The same water, containing cesium in trace concentration ($1 \cdot 10^{-8}$mol/L), was injected at the inlet of the fracture for a short period of time.

Cesium and the other cations sorb onto the available biotite grains via cation exchange. The sorption model (i.e. cation exchange reactions and related selectivity coefficients - see Table 3) is taken from Kyllönen et al. [31], who assumed three different types of ion exchange sites similar to the model of Bradbury and Baeyens [41] for illite: sites on basal planes (95% abundance), interlayer sites on crystal edges (frayed-edge sites, FES) (0.02% abundance) and a third intermediate type site (5% abundance). Considering a mineral density of 3,000 kg/m^3_{min}, the cation exchange capacity of the exchanger is $CEC_{min} = 48.9$ eq/m^3_{min} (subscript min indicates here *mineral*).

Two random uncorrelated realisations of biotite grains were generated. In the first realisation, denoted as Model A (MA) around 8% of the grid cells of the matrix were assumed to contain biotite with a unitary volume fraction (ω [$\mathrm{m}^3_{min}/\mathrm{m}^3_b$], where b stands for *bulk*) whereas in the second realisation (Model B, MB) a twofold biotite content was considered (Figure 7). The distribution of biotite was used to define the bulk cation exchange capacity of each grid cell ($CEC_b = CEC_{min} \cdot \omega$). No sorption sites are available in the fracture.

Snapshots of the distribution of aqueous and sorbed cesium computed with MB after 30 yr from the beginning of the injection are shown in Figure 8. Compared to the non-sorbing tracer (Figure 5), the penetration of cesium is much more limited. The spots with low cesium aqueous concentration and high concentration of cesium in the solid phase correspond to biotite grains.

The cesium breakthrough curves computed for MA and MB are shown in Figure 9. From a simple analysis of these curves, the following conclusion can be drawn:

1. Unlike what was observed for the non-sorbing tracer, both breakthrough curves clearly deviate from the typically expected homogeneous behaviour.
2. The tailing of the breakthrough curves is characterised by a long transition zone, with the slope of the tailing gradually changing from a value of $\sim -1/2$ to the -3/2 slope typically observed in dual porosity systems [8].
3. When less biotite is available in the matrix (MA), a shorter transition zone and a lower level of the late-time tailing is observed.
4. Unlike what is expected considering a homogeneous matrix, at early times no clear separation is observed between the cesium breakthrough curves and the breakthrough curve of the non-sorbing tracer.

5. Compared to the non-sorbing tracer, the cesium breakthrough curves have a lower peak, which is observed at slightly earlier time. This evidence is also in contrast with what is expected when assuming a homogeneous distribution of sorption sites, when the peak of the breakthrough curve is clearly displaced to later times.

5. Upscaling of heterogeneous retention

The sketch of Figure 1 shows a gross representation of the spatial scales that are typically assessed when studying radionuclide transport in fractured media.

Drill cores with isolated fractures are sometimes used to carry out tracer test experiments in the lab [e.g. 42, 43]. This spatial scale is denoted here as *lab-scale* and can be roughly related with a characteristic length of 0.1 to 1 m.

In-situ experiments, such as those mentioned and discussed in sections 1 and 3, are used to investigate e.g. rock matrix retention properties at depth. This scale, denoted as *field-scale*, spans characteristic lengths from 1 to 10 m, approximately.

In safety assessment studies for deep geological disposal of nuclear waste, the scale of interest, denoted here as *site-scale*, has a characteristic length of a few hundred meters to a few kilometers; i.e. the distance travelled by a radionuclide released at repository depth and discharged somewhere in the surface system.

In this chapter we assess how laboratory tracer test data for sorbing nuclides can be upscaled to the *field-scale*. In the next chapter, we also evaluate how the signature of mineralogical heterogeneity propagates and affects radionuclide transport and retention at the *site-scale*.

5.1. Mineralogically heterogeneous models

A single fracture-matrix system of dimension 2.5 m x 0.1 m is discretised using 4,000,000 regular grid cells of size $\delta = 2.5 \cdot 10^{-4}$ m. The fracture is parallel to the x-axis, meaning that its length is 2.5 m. All the parameters describing the system are specified in Table 4. Notice that the models discussed in this section are 2D. A sensitivity analysis to adding the third dimension was carried out and the related results showed no significant change with the results presented hereafter.

Sorption properties in the matrix are described by the following Bernoulli distribution

$$f(k;p) = p^k (1-p)^{1-k} \quad for \quad k \in \{0,1\} \tag{2}$$

where k is the local mineral volume fraction (i.e. volume fraction of the sorbing mineral in the grid cell), which is 1 if the mineral is present and 0 otherwise, and p is the bulk mineral volume fraction in the matrix. If the mineral is present, a linear isotherm sorption model is applied with a distribution coefficient K_d^g=5.3 L/kg, which corresponds to a retardation factor R_g=1,600.

The calculations were carried out in the JURECA booster module [44] of the Jülich Supercomputing Centre using PFLOTRAN. A generic sorbing radionuclide was injected, as a short pulse, at the inlet of the fracture. Two observation points were included, one at a distance of 0.25 m from the fracture inlet and the second at the fracture outlet (2.5 m). The breakthrough curve computed in the first observation point is representative of *lab-scale* while the second observation point simulates a breakthrough curve observed at *field-scale*.

Figure 10 shows the breakthrough curve computed at *lab-scale* for a model with $p = 0.16$. In the same plot, homogeneous breakthrough curves computed using Tang's solution [3] and different retardation values in the matrix are also shown. The breakthrough curve simulated with the 2D mineralogically heterogeneous model is characterised by similar features as those already observed and discussed for the 3D physically and mineralogically heterogeneous models (section 4). For instance, at early times there is no clear separation between the breakthrough curve of the heterogeneous model and the homogeneous solution for a non-sorbing radionuclide (while all the homogeneous curves computed with R>1 are shifted to later times). Also, analogously to what was discussed in section 4, the tailing of the heterogeneous breakthrough curve is characterised by a transition zone with the slope (log-log scale) being first very smooth and then approaching gradually the -3/2 slope.

The results obtained at *field-scale* (Figure 11) point out that the signature of mineralogical heterogeneity propagates and has a significant effect over larger scales. Although the shape of the heterogeneous breakthrough curve is now smoothed out and the transition in the slope is no longer evident, the curve still exhibits a significant early arrival and an anomalous rising limb. Interestingly, the declining limb of the curve is reasonably well described by the homogeneous solution with $K_d = K_d^g \cdot p$. However, as for the *lab-scale*, none of the homogeneous solutions are able to capture the full shape of the curve. The need to investigate how the heterogeneous signal propagates over larger spatial scales and practical limitations to further extend the heterogeneous mechanistic models motivates the development of upscaling strategies, which are detailed in the next two sub-sections.

5.2. Upscaling strategy I: Direct Sampling (DS) of the Retention Time Distribution (RTD)

The two upscaling approaches proposed hereafter make use of standard concepts used in time domain random walk (TDRW) methods. The calculations presented hereafter were carried out using the computer code MARFA [15, 45].

The basic spatial unit used here is defined as a *segment*. A segment is typically associated to a part of a particle pathline that lies in a fracture and is delimited by the intersection with two adjacent fractures. Nevertheless, this definition is not stringent, meaning that different and alternative conceptual representations of a segment can be envisaged. Here, we define a segment as the fracture length sampled by a *lab-scale* tracer test experiment.

The unit response of a *lab-scale* tracer test can be expressed as [15]:

$$f_{tran}(t) = \int_0^\infty \int_0^\infty f_{ret}(t-\tau|\,\beta) f_{\beta|\tau}(\beta|\,\tau) f_\tau(\tau) d\tau d\beta \tag{3}$$

where τ [y] is the groundwater travel time in the fracture segment, with related probability density function f_τ, $t-\tau = t_{ret} \geq 0$ is the retention time in the matrix and f_{ret} is its corresponding probability density function, denoted here as *retention time distribution* and β [y/m] is a hydrodynamic control parameter denoted as *transport resistance*, defined as [e.g. 7]:

$$\beta(\tau) = \int_0^\tau \frac{d\theta}{b(\theta)} \tag{4}$$

where b [m] is the fracture half aperture and θ is the variable of integration. The integration is along the segment. Notice that β and τ are strongly correlated, which explains why the distribution of β is conditional on τ.

We consider here a simplified model, denoted with superscript *SM*, characterised by $f_\tau = \delta(\tau - \tau_0)$ and $b = b_0$. For this model the following relationship holds:

$$f_{tran}^{SM}(t) = f_{ret}^{SM}(t - \tau_0) \tag{5}$$

By equating Equations 5 and 3, we obtain an equivalent retention time distribution, which can be seen as a non-parameteric function that lumps together all the random processes that might affect a particle; i.e. in-plane dispersion, matrix diffusion and retention into either fracture surface or in the rock matrix. f_{ret}^{SM} can be directly inferred from the lab-scale breakthrough curve, this is why the proposed approach is denoted as *Direct Sampling (DS) approach*. f_{ret}^{SM} is then used in TDRW simulations to route particles along pathlines made-up of N segments, under the basic premise that each segment is characterised by the same hydrodynamic processes (i.e. same distribution of τ and β).

The practical implementation of the upscaling exercise is carried out using the following stepwise approach:

1. The breakthrough curve of the sorbing radionuclide obtained at 0.25 m distance from the inlet (Figure 10) is used to extract f_{ret}^{SM}.
2. For the i-th particle, the retention time, $t_{ret} = t_{tran} - \tau_0$ is sampled from f_{ret}^{SM} and the particle clock is set to $t_{clk,i}^{j} = t_{clk,i}^{j-1} + t_{ret} + \tau_0$. Notice that index j indicates the fracture segment and that $t_{clk,i}^{0} = 0$; i.e. the particle clock is set to 0 at the inlet segment.
3. For the i-th particle, step 2 is repeated ten times until obtaining the particle arrival time, $t_{ar,i}$, at the end of a pathline of length 2.5 m.

The cumulative breakthrough curve is computed from all the particle arrival times and the instantaneous breakthrough curve is reconstructed using a kernel-based method [15]. The result of the TDRW simulation are compared with the breakthrough curve obtained using PFLOTRAN at a distance of 2.5 m from the inlet (Figure 11).

The results of the exercise are shown in Figure 12. The small fluctuations observed in the MARFA solution at late times are related to statistical noise intrinsic in particle-based Monte Carlo methods. Yet, the agreement between the breakthrough curve computed with MARFA and the synthetic solution obtained with PFLOTRAN is very good, which indicates that the heterogeneous signal observed at *lab-scale* and affected by heterogeneous retention can be extracted and successfully convoluted at larger scale. This evidence motivates the development of a parameteric upscaling strategy (next sub-section) that has a broader application and is not only limited to pathlines with fixed fracture aperture.

5.3. Upscaling strategy II: three parallel pathway model (TPPM)

Different analytical solutions were derived for f_{ret} [e.g. 3, 4, 16]. Here we will use the simplest solution, which is based on the assumption of a homogeneous infinite matrix [3] and which expresses the retention time distribution as

$$f_{ret} = \frac{\mathcal{H}(t_{ret})\kappa\beta}{2\sqrt{\pi}t_{ret}^{3/2}} \exp\left(\frac{-\kappa^2\beta^2}{4t_{ret}}\right) \tag{6}$$

where $\mathcal{H}()$ is the Heaviside function. In Equation 6, κ [(m^2/y)$^{0.5}$] is a material parameter group defined as $\kappa = \phi\sqrt{D_e R} = \sqrt{D_p \phi^3 R}$.

We assume here that mass discharge at the fracture outlet is the linear combination of three parallel pathways:

$$f_{tran}(t) = \alpha f_{tran}^{ns}(t) + \beta f_{tran}^{ms}(t) + \gamma f_{tran}^{hs}(t) \tag{7}$$

where f_{tran} is defined as in Equation 3 and α, β and γ [-] are three coefficients that provide the relative amount of mass that is routed through each of the three pathways. Mass conservation is ensured by setting

$$\alpha + \beta + \gamma = 1 \tag{8}$$

The three pathways are characterised by the same transport resistance, while κ varies as each pathway is characterised by different retention properties: in the non-sorbing pathway (superscript *ns*) there is no sorption (R=1), in the mildy sorbing pathway (superscript *ms*) retardation is equal to half of the retardation in the mineral grains (R=R$_g$/2) whereas in the highly sorbing pathway (superscript *hs*) R=R$_g$. The corresponding retention time distributions are defined as f_{ret}^{ns}, f_{ret}^{ms} and f_{ret}^{hs}. No mass exchange is considered between pathways.

Before discussing details of the upscaling approach, it is worthwhile noting that evidence of a similar composite behaviour of the heterogeneous rock matrix has been found in different laboratory and field experiments [46, 47, 19]. Moreover, Iraola et al. [13] recently used a two-parallel pathways model to qualitatively interpret results of the LTDE-SD experiment whereas Trinchero et al. [48] pointed out that the transport of oxygen in a granitic rock is characterised by a composite behaviour, with the average oxygen penetration profile being the result of multiple parallel diffusive pathway characterised by different "reactivity".

The three-parallel pathway model (TPPM) was implemented in MARFA using a conditional sampling scheme explained in detail in Appendix A.

The models used in this upscaling exercise are analogous to that used in section 5.2 and illustrated in section 5.1, however here different mineral distributions are considered, which span from $p = 0.04$ to $p = 0.5$; i.e. respectively 4% and 50% of sorbing mineral volume fraction. The exercise is carried out using a stepwise approach:

- Step 1 (calibration): the breakthrough curves of the *lab-scale* experiments are best fitted using MARFA and the TPPM. A single segment is used and the best fit is performed by mean squared error minimisation.
- Step 2 (validation): for each considered mineral distribution, the coefficients estimated in step 1 are used to run a MARFA calculation with the TPPM and 10 equally spaced segments. The results of step 2 are compared with the breakthrough curves obtained using PFLOTRAN and the related mineral distribution at a distance of 2.5 m from the inlet.

The results of step 1 are shown in Figure 13 and the coefficients estimated for each considered mineral distribution are plotted in Figure 14. The TPPM model describes well the *lab-scale* breakthrough curves, which indicates that, consistently with what was observed in previous studies [e.g. 12, 13, 48], the medium indeed behaves as a composite system. Until a volume fraction of the sorbing mineral of around 15%, the system is fairly well approximated by a dual parallel pathway model built as a linear combination of the non-sorbing and the mildly sorbing pathway. For a higher amount of sorbing mineral, an additional degree of freedom (i.e. the highly sorbing pathway) is needed to properly capture the composite behaviour of the medium.

The results of step 2 are shown in Figure 15. Slight differences between the PFLOTRAN and MARFA solutions are observed in the rising limb of the breakthrough curve computed for a very low amount of sorbing mineral ($p = 0.04$). For all the other breakthrough curves, the agreement between the synthetic experiment and the upscaled solution is very good. This suggests that, as already observed in section 5.2, when the signal of a *lab-scale* experiment affected by heterogeneous retention is properly captured, it can then be successfully propagated along the pathway to describe the signal over a much larger scale.

6. Large-scale modelling

6.1. Models with constant transport properties

In sections 5.2 and 5.3 we have demonstrated that the signal observed in a tracer test analysed at *lab-scale* and affected by heterogenous retention can be extracted and propagated over larger scales. In this section, we take advantage of this methodological approach to investigate the effect that heterogeneous retention in the matrix, due to the sparse availability of sorption sites, has on radionuclide transport at *site-scale*; i.e. the scale of interest in a safety assessment study for a deep geological repository for nuclear waste.

We consider a pathline of 250 m length constituted by 1000 fracture segments of 0.25 m length. Each fracture segment and the surrounding matrix are described by the parameters in Table 4. It is also assumed that the amount of sorbing mineral is $p = 0.16$. The propagation of the heterogeneous signal is done using TPPM. Notice that analogous results have been obtained using the DS approach (results are not shown here for the sake of brevity).

The heterogeneous breakthrough curve is compared with three homogeneous calculations: one, where no sorption is included, a second, where homogeneous retention is set with R=1,600, and a third with R=250 (i.e. $K_d = K_d^g \cdot p$) in the whole matrix. The comparison of the different breakthrough curves is shown in Figure 16. At large-scale the heterogeneous signature is no longer evident. As already noticed in the previous sections, the breakthrough curve computed with the homogeneous model and with R=1,600 (i.e. retardation equal to retardation in the pure mineral phase) strongly overestimates the retardation capacity of the matrix. Interestingly, the heterogenous breakthrough curve is very well described by a model where the distribution coefficient in the pure mineral phase is scaled by the mineral volume fraction.

6.2. Spatial persistence of the heterogeneous signature

We have discussed earlier that, at small scale, the sparse distribution of mineral grains leads to a heterogeneous signature, which affects the early part (rising limb) of the breakthrough curves of sorbing radionuclides. At large scale the deviation from the homogeneous-based solution is smoothed out. We aim at assessing here the spatial persistence of this heterogeneous signature. To this end, the five different mineral distributions of section 5.3 are considered (i.e. $p = 0.04$ to $p = 0.5$). For each mineral distribution the TPPM model is run with the related coefficients (see Figure 14) along a pathline made up of N equally time spaced segments, each segment being equal to the *lab-scale* model of section 5.1. These models are here denoted as *heterogeneous models*. A corresponding homogeneous calculation (*homogeneous model* from now on) was also run with $K_d = K_d^g \cdot p$ and the relative difference in the first arrival time was computed as $(t_{hom} - t_{het})/t_{het}$ where t_{hom} and t_{het} [T] is the time when 1% of the total injected mass reaches the considered segment outlet for the homogeneous and heterogeneous model, respectively.

Figure 17 shows the relative error in the estimate of the first arrival time as a function of cumulative β, for the five considered mineral distributions. It is interesting to notice that, for a high amount of sorbing mineral (e.g. $p = 0.5$), the homogeneous model largely over-predicts the first arrival time at small scales but the solution approaches the homogeneous breakthrough curves at relatively short distances. For a small amount of sorbing mineral, the error at small scales is lower but the spatial persistence of the heterogeneous signature is much longer; e.g. errors above 20% for $\beta \leq 50,000$ y/m.

At large scales the results of all the tested heterogeneous models approach those of the equivalent homogeneous models, although a slightly negative error is observed as the homogeneous model slightly under-predicts the early arrival time; see e.g. the rising limb of the two curves in Figure 16.

The significance of biotite for the retention of potentially harmful radionuclides, particularly cesium (e.g., Cs-137 and Cs-135) and sodium, has been discussed early in this manuscript. At Forsmark biotite is found to be present in a relatively low amount: e.g. from 0.8 to 8 vol% in granitic rock [32]. In the last Swedish safety analysis for a deep geological repository for spent nuclear fuel (SR-Site), typical values of cumulative β associated with failing canisters varied from about $1.5 \cdot 10^4$ y/m to 10^5 y/m [49]. It turns out that the significantly long persistence of the heterogeneous signature pointed out in this work might have implications for calculations of radionuclide transport carried out at the scale of a typical safety assessment study.

6.3. Models based on different transport classes

Radionuclide transport calculations carried out at the *site-scale* entail the need to account for different rock types [32] that are characterised by specific retention properties, which are in turn related to the different mineralogical properties of the considered lithological units [50]. This heterogeneity is typically treated by defining a finite number of transport classes, with related retention properties, that are sampled statistically conditioned on the lithological unit to which the given fracture segment belongs [e.g. 51].

Here, the effect of longitudinal heterogeneity is assessed in an idealised way by defining five simplified transport classes characterised by different amount of sorbing mineral: TC1 with $p = 0.04$, TC2 with $p = 0.08$, TC3 with $p = 0.16$, TC4 with $p = 0.32$ and TC5 with $p = 0.5$. The transport calculation is carried along a pathline made up of 1000 equally time spaced segments, each segment being equal to the *lab-scale* model of section 5.1. Furthermore, each segment is related to one of the five transport classes and the TPPM is used, with the coefficients shown in Figure 14.

The five different transport classes were distributed along the considered transport pathway using a sequential indicator simulation that was carried out with the computer code SGeMS [52]. Equal fractions of each transport class were considered (i.e. 20% each), which gives an average amount of sorbing mineral equal to $< p >= 0.22$. A spherical isotropic semivariogram, with a range equal to 10 m was used. An additional case was also included in the analysis, in which the same proportion of transport classes was distributed in an uncorrelated way along the pathway. The two resulting distributions of transport classes are shown in Figure 18. The two models are here defined as *correlated* and *uncorrelated* models.

In Figure 19, the breakthrough curve computed with the *correlated* model is compared with the related breakthrough curves obtained using three different homogeneous models: one where sorption in the matrix is assumed to be equal to sorption in the pure mineral phase ($R = 1,600$), a second where no sorption in the matrix is considered and a third where the distribution coefficient is scaled by the average mineral volume fraction: $K_d = K_d^g \cdot < p >$ (i.e. $R = 352$). Results are very similar to those already discussed in section 6.1: the model with no sorption and the model with sorption equal to sorption in the pure mineral phase, respectively, significantly underestimate and overestimate the retention capacity of crystalline rocks. On the contrary, the equivalent homogeneous model based on the distribution coefficient scaled by the average mineral volume fraction (arithmetic mean) provides a good approximation to the heterogeneous solution, although the rising limb of the curve is displaced to earlier times. A similar slight underestimation of the early arrival was already discussed in the previous section (see also Figure 17).

The results of the correlated and the uncorrelated heterogeneous models were almost identical (results not shown here), which indicates that longitudinal correlation in transport classes has a modest effect on radionuclide transport. This finding provides support for the methodology employed in previous safety cases to populate fracture segments with transport classes sampled statistically without considering any spatial correlation [see e.g. 51].

7. Discussion

Micro-characterisation studies, based on e.g. micro-computed tomography or digital autoradiography, have pointed out that in granitic rocks sorbing minerals are sparsely distributed and this heterogeneous distribution leads to diffusion patterns that differ from what is typically predicted by homogeneous-based models. This heterogeneous behaviour has been observed in different in-situ diffusion experiments.

The available experimental evidence has led us to formulate three research questions (see section 2). Based on the results of this work, the following answers can be given: (i) at small scale, the sparse distribution of sorption sites, which is intrinsically related to the underlying micro-scale heterogeneity, has a significant impact on diffusive patterns leading to heterogeneous breakthrough curves for sorbing radionuclides, (ii) these heterogeneous breakthrough curves can be used to infer non-parameteric retention time distribution functions or, alternatively, to calibrate the parameters of a model based on parallel diffusive pathways that account for the underlying micro-scale heterogeneity, and (iii) at large scale, the heterogeneous breakthrough curves are smoothed out and the breakthrough curves of sorbing radionuclides are well described by homogeneous solutions based on equivalent distribution coefficients.

The proposed upscaling procedures are based on idealised segmented pathways characterised by constant hydrodynamic properties (i.e. τ and β). Real fracture systems are obviously much more complex and might show strong contrasts in velocity and aperture between nearby fractures [e.g. 25]. Moreover, fractures might have experienced different hydrothermal alteration events that could have altered the properties of the rock matrix close the flowing fracture. Therefore, additional work is needed to make the proposed framework applicable to study contaminant transport in large-scale fractured media. A possible approach would be to use a piecewise-approximation in which fracture segments are grouped into transport classes and the related RTD functions are derived from reactive transport models as shown in section 5.1. A similar approach based on transport classes was used in the in last Finnish safety assessment study of Olkiluoto, the designated location for a repository of spent nuclear fuel, to account for different radionuclide retention properties of different types of rock matrices [53]. However, it is worthwhile pointing out here that one of the main outcomes of this work is that at large-scale the heterogeneous and sparse availability of sorption sites can be well described by an equivalent distribution coefficient. This simple yet practical approach is of direct relevance for any existing radionuclide transport model in fractured crystalline rock.

Another pending task is to elucidate the mutual interplay between fracture internal aperture heterogeneity and heterogeneous retention which could be done by combing theoretical models [e.g. 54] with direct simulations. The simulations would focus on resolving both the complex topology of a real fracture and the surrounding rock matrix, which in turn should include an explicit description of the sparsely distributed sorption sites.

8. Summary and conclusions

In the first part of this work we have presented a detailed process-based simulation of a radionuclide tracer test in a synthetic fracture-matrix system to analyse the influence of micro-scale heterogeneity on breakthrough curves of sorbing radionuclides. The results of the reactive transport simulations point out that at small scale (e.g. the scale representative of a laboratory tracer test experiment) the breakthrough curve is characterised by a shape that significantly differs from homogeneous-based solutions, with a very early arrival and a smooth slope of the tailing at intermediate times. This heteorgeneous signature is caused by the sparse distribution of sorption sites.

Starting from this evidence and using a formulation based on retention time distributions we have provided two different upscaling strategies. The main general conclusions can be summarised as follows:

1. The heterogeneous radionuclide breakthrough curve observed at small scale (e.g. *lab-scale*) can be used to extract the radionuclide retention time distribution in the matrix.
2. Using the retention time distribution extracted from point 1, the heterogeneous signal can be successfully propagated along larger scale.
3. At large scales (e.g. *site-scale*) the heterogeneous signature of the smal-scale signal is smoothed out and the breakthrough curve is well approximated by a homogeneous model in which the distribution coefficient of the sorbing mineral grains is scaled by the mineral volume fraction.
4. The heterogeneous signature is shown to persist, particularly when the sorbing mineral is present in low amount.

Changes in retention properties along a transport pathway have also been assessed by defining simplified transport classes characterised by different amount of sorbing mineral. The results of these longitudinally heterogeneous models have shown that, at large scale, the resulting radionuclide breakthrough curve can fairly well be described by an equivalent homogeneous model based on the distribution coefficient of the pure mineral phase scaled by the average amount of sorbing mineral along the pathway. The spatial correlation of the different transport classes along the transport pathway was shown to have a negligible effect on the results.

Acknowledgements PT and VC thank the Swedish Nuclear Fuel and Waste Management Company (SKB) for the financial support. DB and GD acknowledge financial support provided by the German Federal Ministry of Education and Research (BMBF, grant agreement 02NUK053A) and the Initiative and Networking Fund of the Helmholtz Association (HGF grant SO-093) within the collaborative project iCross. The authors gratefully acknowledge the computing time granted through JARA on the supercomputers JUQUEEN and JURECA at Forschungszentrum Jülich. The paper has benefited from insightful comments by Johan Byegård, Henrik Drake, Kersti Nilsson, Marja Siitari-Kauppi and three anonimous reviewers.

References

[1] Fried, S., Friedman, A.M., Atcher, R., Hines, J.. Retention of plutonium and americium by rock. Science 1977;196(4294):1087–1089.

[2] Neretnieks, I.. Diffusion in the rock matrix: an important factor in radionuclide retardation. Journal of Geophysical Research 1980;85(B8):4379–4397.

[3] Tang, D., Frind, E., Sudicky, E.A.. Contaminant transport in fractured porous media: Analytical solution for a single fracture. Water Resources Research 1981;17(3):555–564.

[4] Sudicky, E.A., Frind, E.. Contaminant transport in fractured porous media: Analytical solution for a system of parallel fractures. Water Resources Research 1982;18(3):1634–1642.

[5] Haggerty, R., Gorelick, S.M.. Multiple-rate mass transfer for modeling diffusion and surface reactions in media with pore-scale heterogeneity. Water Resources Research 1995;31(10):2383–2400.

[6] Carrera, J., Sánchez-Vila, X., Benet, I., Medina, A., Galarza, G., Guimerà, J.. On matrix diffusion: formulations, solution methods and qualitative effects. Hydrogeology Journal 1998;6(1):178–190.

[7] Cvetkovic, V., Selroos, J., Cheng, H.. Transport of reactive tracers in rock fractures. Journal of Fluid Mechanics 1999;378:335–356.

[8] Haggerty, R., McKenna, S.A., Meigs, L.C.. On the late-time behavior of tracer test breakthrough curves. Water Resources Research 2000;36(12):3467–3479.

[9] Hellmuth, K., Siitari-Kauppi, M., Lindberg, A.. Study of porosity and migration pathways in crystalline rock by impregnation with 14c-polymethylmethacrylate. Journal of Contaminant Hydrology 1993;13(1):403 – 418. URL: `http://www.sciencedirect.com/science/article/pii/0169772293900732`. doi:`https://doi.org/10.1016/0169-7722(93)90073-2`; chemistry and Migration of Actinides and Fission Products.

[10] Siitari-Kauppi, M.. Development of 14c-polymethylmethacrylate method for the characterisation of low porosity media. Application to Rocks in Geological Barriers of Nuclear Waste Storage [Ph D thesis]: Helsinki, Finland, University of Helsinki, Report Series in Radiochemistry 2002;17:156.

[11] Sardini, P., Robinet, J., Siitari-Kauppi, M., Delay, F., Hellmuth, K.. Direct simulation of heterogeneous diffusion and inversion procedure applied to an out-diffusion experiment. test case of palmottu granite. Journal of Contaminant Hydrology 2007;93(1):21–37.

[12] Robinet, J.C., Sardini, P., Delay, F., Hellmuth, K.H.. The effect of rock matrix heterogeneities near fracture walls on the residence time distribution (rtd) of solutes. Transport in Porous Media 2008;72(3):393–408. URL: `https://doi.org/10.1007/s11242-007-9159-7`.

[13] Iraola, A., Trinchero, P., Voutilainen, M., Gylling, B., Selroos, J.O., Molinero, J., et al. Microtomography-based Inter-Granular Network for the simulation of radionuclide diffusion and sorption in a granitic rock. Journal of Contaminant Hydrology 2017;207:8–16. doi:`10.1016/j.jconhyd.2017.10.003`.

[14] Voutilainen, M., Kekäläinen, P., Siitari-Kauppi, M., Sardini, P., Muuri, E., Timonen, J., et al. Modeling transport of cesium in grimsel granodiorite with micrometer scale heterogeneities and dynamic update of kd. Water Resources Research 2017;53(11):9245–9265. URL: `https://agupubs.onlinelibrary.wiley.com/doi/abs/10.1002/2017WR020695`. doi:`10.1002/2017WR020695`. `arXiv:https://agupubs.onlinelibrary.wiley.com/doi/pdf/10.1002/2017WR020695`.

[15] Painter, S., Cvetkovic, V., Mancillas, J., Pensado, O.. Time domain particle tracking methods for simulating transport with retention and first-order transformation. Water Resources Research 2008;44(1)(1).

[16] Cvetkovic, V.. Significance of fracture rim zone heterogeneity for tracer transport in crystalline rock. Water Resources Research 2010;46(3).

[17] Trinchero, P., Painter, S., Ebrahimi, H., Koskinen, L., Molinero, J., Selroos, J.O.. Modelling radionuclide transport in fractured media with a dynamic update of kd values. Computers & Geosciences 2016;86:55–63.

[18] Winberg, A., Andersson, P., Byegård, J., Poteri, A., Cvetkovic, V., Dershowitz, W., et al. Final report of the true block scale project. Tech. Rep. TR-02-16; Svensk Kärnbränslehantering AB (SKB), Stockholm, Sweden; 2003.

[19] Nilsson, K., Byegård, J., Selnert, E., Widestrand, H., Höglund, S., Gustafsson, E.. Äspö hard rock laboratory. Long Term Sorption Diffusion Experiment (LTDE-SD). Results from rock sample analyses and modelling. Tech. Rep. R-10-68; Svensk Kärnbränslehantering AB, Stockholm, Sweden; 2010.

[20] Timonen, J., Koskinen, L.. The first matrix diffusion experiment in the water phase of the repro project: Wpde1. Tech. Rep. Working Report 2017-23; Posiva OY, Euroajoki, Finland.; 2018.

[21] Hadermann, J., Heer, W.. The Grimsel (Switzerland) migration experiment: integrating field experiments, laboratory investigations and modelling. Journal of Contaminant Hydrology 1996;21(1-4):87–100.

[22] Vilks, P., Cramer, J., Jensen, M., Miller, N., Miller, H., Stanchell, F.. In situ diffusion experiment in granite: phase i. Journal of Contaminant Hydrology 2003;61(1):191–202.

[23] Carslaw, H., Jaeger, J.. Conduction of heat in solids. Oxford: Clarendon Press, 2nd ed 1959;1.

[24] Posiva Oy, . Olkiluoto site description 2011. Tech. Rep. POSIVA Report 2011-02; Posiva OY, Helsinki, Finland.; 2013.

[25] SKB, . Site-descriptive modelling for a final repository for spent nuclear fuel in Sweden. Main report of the SR-Site project. Tech. Rep. TR-11-01; Svensk Kärnbränslehantering AB, Stockholm, Sweden.; 2013.

[26] Voutilainen, M., Siitari-Kauppi, M., Sardini, P., Lindberg, A., Timonen, J.. Porespace characterization of an altered tonalite by x-ray computed microtomography and the 14c-labeled-polymethylmethacrylate method. Journal of Geophysical Research 2012;117. B01201.

[27] Svensson, U., Löfgren, M., Trinchero, P., Selroos, J.O.. Modelling the diffusion-available pore space of an unaltered granitic rock matrix using a micro-DFN approach. Journal of Hydrology 2018;559. URL: `http://www.sciencedirect.com/science/article/pii/S0022169418301161`.

[28] Sidborn, M., Neretnieks, I.. Long-term oxygen depletion from infiltrating groundwaters: Model development and application to intra-glaciation and glaciation conditions. Journal of Contaminant Hydrology 2008;100(1):72–89.

[29] MacQuarrie, K., Mayer, K., Jin, B., Spiessl, S.. The importance of conceptual models in the reactive transport simulation of oxygen ingress in sparsely fractured crystalline rock. Journal of Contaminant Hydrology 2010;112(1):64–76.

[30] Trinchero, P., Puigdomenech, I., Molinero, J., Ebrahimi, H., Gylling, B., Svensson, U., et al. Continuum-based DFN-consistent numerical framework for the simulation of oxygen infiltration into fractured crystalline rocks. Journal of Contaminant Hydrology 2017;200:60–69. doi:`10.1016/j.jconhyd.2017.04.001`.

[31] Kyllönen, J., Hakanen, M., Lindberg, A., Harjula, R., Vehkamäki, M., Lehto, J.. Modeling of cesium sorption on biotite using cation exchange selectivity coefficients. Radiochimica Acta 2014;102(10):919–929.

[32] Drake, H., Sandström, B., Tullborg, E.. Mineralogy and geochemistry of rocks and fracture fillings from Forsmark and Oskarshamn: Compilation of data for SR-Can. Tech. Rep. R-06-109; Svensk Kärnbränslehantering AB (SKB), Stockholm, Sweden; 2006.

[33] Widestrand, H., Byegård, J., Selnert, E., Skålberg, M., Höglund, S., Gustafsson, E.. Long term sorption diffusion experiment (LTDE-SD). Supporting laboratory program — Sorption diffusion experiments and rock material characterisation. Tech. Rep. R-10-66; Svensk Kärnbränslehantering AB, Stockholm, Sweden; 2010.

[34] Svensson, U., Kuylenstierna, H.O., Ferry, M.. DarcyTools version 3.4: concepts, methods and equations. Tech. Rep. R-07-38; Svensk Kärnbränslehantering AB (SKB), Stockholm, Sweden; 2010.

[35] Svensson, U., Ferry, M.. Darcytools: A computer code for hydrogeological analysis of nuclear waste repositories in fractured rock. Journal of Applied Mathematics and Physics 2014;2(06):365.

[36] Svensson, U.. A continuum representation of fracture networks. Part I: Method and basic test cases. Journal of Hydrology 2001;250(1):170–186.

[37] Svensson, U.. A continuum representation of fracture networks. Part II: Application to the Äspö Hard Rock laboratory. Journal of Hydrology 2001;250(1):187–205.

[38] Stephan, M., Docter, J.. JUQUEEN: IBM Blue Gene/Q Supercomputer System at the Jülich Supercomputing Centre. Journal of large-scale research facilities JLSRF 2015;1(http://dx.doi.org/10.17815/jlsrf-1-18).

[39] Lichtner, P., Hammond, G., Lu, C., Karra, S., Bisht, G., Andre, B., et al. PFLOTRAN Web page. 2013. Http://www.pflotran.org.

[40] Hammond, G., Lichtner, P., Mills, R.. Evaluating the performance of parallel subsurface simulators: An illustrative example with PFLOTRAN. Water Resources Research 2014;50(1):208–228.

[41] Bradbury, M.H., Baeyens, B.. A generalised sorption model for the concentration dependent uptake of caesium by argillaceous rocks. Journal of Contaminant Hydrology 2000;42(2):141–163.

[42] Hölttä, P., Poteri, A., Siitari-Kauppi, M., Huittinen, N.. Retardation of mobile radionuclides in granitic rock fractures by matrix diffusion. Physics and Chemistry of the Earth, Parts A/B/C 2008;33(14):983 – 990. URL: `http://www.sciencedirect.com/science/article/pii/S1474706508001095`. doi:`https://doi.org/10.1016/j.pce.2008.05.010`; mIGRATION 2007, 11th International Conference on the Chemistry and Migration Behaviour of Actinides and Fission Products in the Geosphere.

[43] Tachi, Y., Ito, T., Akagi, Y., Satoh, H., Martin, A.J.. Effects of fine-scale surface alterations on tracer retention in a fractured crystalline rock from the grimsel test site. Water Resources Research 2018;0(0). URL: `https://agupubs.onlinelibrary.wiley.`

com/doi/abs/10.1029/2018WR023145. doi:10.1029/2018WR023145. arXiv:https://agupubs.onlinelibrary.wiley.com/doi/pdf/10.1029/2018WR023145.

[44] Jülich Supercomputing Centre, . JURECA: Modular supercomputer at Jülich Supercomputing Centre. Journal of large-scale research facilities 2018;4(A132). URL: http://dx.doi.org/10.17815/jlsrf-4-121-1. doi:10.17815/jlsrf-4-121-1.

[45] Painter, S., Mancillas, J.. Marfa user's manual: Migration analysis of radionuclides in the far field. Tech. Rep. POSIVA Working Report 2013-01; Posiva Oy, Helsinki, Finland.; 2013.

[46] Tsukamoto, M., Ohe, T.. Effects of biotite distribution on cesium diffusion in granite. Chemical Geology 1993;107(1):29 – 46. URL: http://www.sciencedirect.com/science/article/pii/000925419390100W. doi:https://doi.org/10.1016/0009-2541(93)90100-W.

[47] Johansson, H., Siitari-Kauppi, M., Skålberg, M., Tullborg, E.L.. Diffusion pathways in crystalline rock - examples from Äspö-diorite and fine-grained granite. Journal of Contaminant Hydrology 1998;35(1–3):41–53.

[48] Trinchero, P., Sidborn, M., Puigdomenech, I., Svensson, U., Ebrahimi, H., Molinero, J., et al. Transport of oxygen into granitic rocks: Role of physical and mineralogical heterogeneity. Journal of Contaminant Hydrology 2018;URL: http://www.sciencedirect.com/science/article/pii/S0169772218303838. doi:https://doi.org/10.1016/j.jconhyd.2018.12.001.

[49] SKB, . Radionuclide transport report for the safety assessment sr-site. Tech. Rep. TR-10-50; Svensk Kärnbränslehantering AB (SKB), Stockholm, Sweden; 2010.

[50] Crawford, J.. Bedrock transport properties Forsmark: site descriptive modelling SDM-Site Forsmark. Tech. Rep. R-08-48; Svensk Kärnbränslehantering AB (SKB), Stockholm, Sweden; 2008.

[51] Hartley, L., Baxter, S., Hoek, J., Mosley, K., Williams, T., Fox, A., et al. Discrete Fracture Network Modelling (Version 3) in Support of Olkiluoto Site Description 2018. Tech. Rep. WR 2017-32; Posiva OY, Helsinki, Finland; 2018.

[52] Remy, N., Boucher, A., Wu, J.. Applied geostatistics with SGeMS: a user's guide. Cambridge University Press; 2009.

[53] Posiva Oy, . Safety case for the disposal of spent nuclear fuel at olkiluoto. Tech. Rep. POSIVA report 2012-07; Posiva OY, Helsinki, Finland.; 2012.

[54] Cvetkovic, V., Cheng, H.. Sorbing tracer experiments in a crystalline rock fracture at Äspö (sweden): 3. effect of microscale heterogeneity. Water Resources Research 2008;44(12). URL: `https://agupubs.onlinelibrary.wiley.com/doi/abs/10.1029/2007WR006797`. doi:10.1029/2007WR006797. `arXiv:https://agupubs.onlinelibrary.wiley.com/doi/pdf/10.1029/2007WR006797`.

Parameter	Set 1	Set 2	Set 3
Length interval [mm]	5-20	4-5	1-2
Intensity I [m^{-3}]	0.60	100	500
Aperture [m]	$5 \cdot 10^{-7}$	$5 \cdot 10^{-7}$	$5 \cdot 10^{-7}$
Intrinsic local tortuosity τ_D^l [-]	$\sqrt{5}$	$\sqrt{5}$	$\sqrt{5}$
Power law exponent a [-]	-2.6	-2.6	-2.6
Fracture centre orientation	Poisson	Poisson	Close to 4-5 mm set
Fracture normal vector orientation	Poisson	Poisson	Poisson

Table 1: Input data used to generate the heterogeneous matrix.

Groundwater composition	
pH	7.3
Total concentration (mol/L)	
Na^{+}	$3.3 \cdot 10^{-2}$
K^{+}	$6.1 \cdot 10^{-4}$
Ca^{2+}	$9.5 \cdot 10^{-4}$
Cl^{-}	$3.1 \cdot 10^{-2}$
SO_4^{2-}	$2.1 \cdot 10^{-3}$

Table 2: Chemical composition of the groundwater used in the reactive transport calculations.

Reaction	Selectivity coefficients ($\log K$)
Planar sites	
$X^- + Na^+ \leftrightarrow NaX$	0.0
$X^- + K^+ \leftrightarrow KX$	2.3
$X^- + Cs^+ \leftrightarrow CsX$	2.0
Intermediate sites	
$X^-_{int} + Na^+ \leftrightarrow NaX_{int}$	0.0
$X^-_{int} + K^+ \leftrightarrow KX_{int}$	2.3
$X^-_{int} + Cs^+ \leftrightarrow CsX_{int}$	4.5
Frayed-edge sites	
$X^-_{FES} + Na^+ \leftrightarrow NaX_{FES}$	0.0
$X^-_{FES} + K^+ \leftrightarrow KX_{FES}$	2.5
$X^-_{FES} + Cs^+ \leftrightarrow CsX_{FES}$	8.0

Table 3: Cation exchange reactions and selectivity coefficients (Gaines-Thomas convention) [31].

Parameter	Value
Half fracture spacing (δ_m)	0.1 m
Half fracture aperture (δ_f)	$0.25 \cdot 10^{-3}$ m
Pore diffusion coefficient (D_p)	$3.5 \cdot 10^{-13}$ m^2/s
Matrix porosity (ϕ)	$1.0 \cdot 10^{-2}$
Rock density (ρ)	$3.0 \cdot 10^3$ kg/m^3
Fracture water volumetric flux ($\|\boldsymbol{q}_f\|$)	$1.0 \cdot 10^{-8} m/s$

Table 4: Parameters for the single fracture-matrix system.

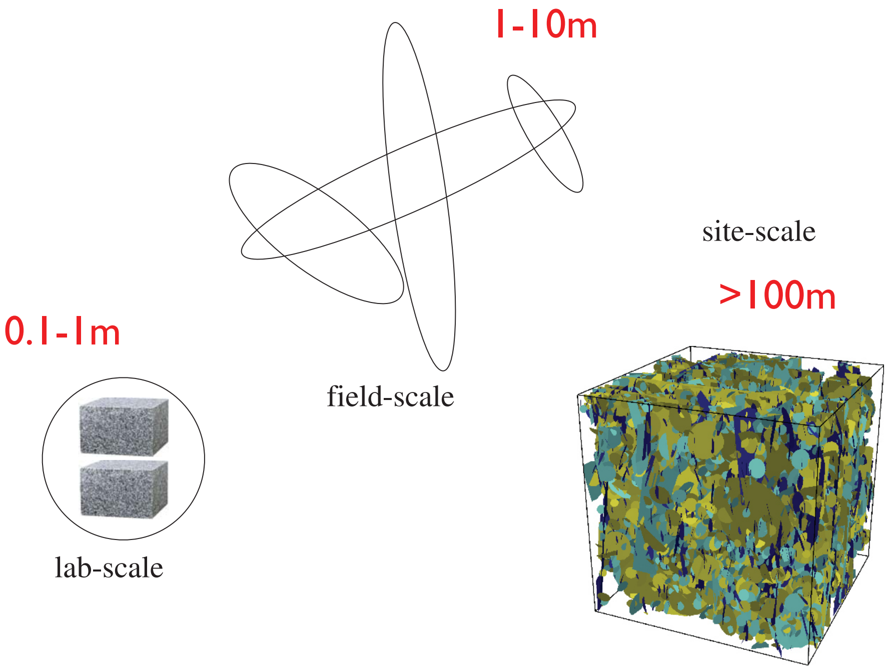

Figure 1: Sketch showing the different spatial scales considered when assessing radionuclide transport in fractured rock.

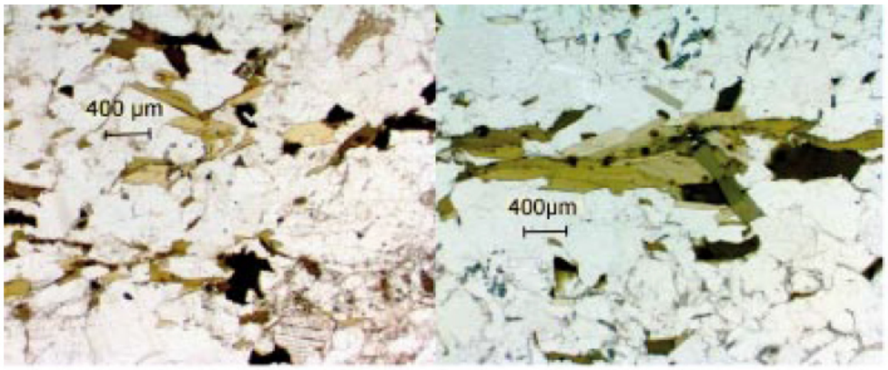

Figure 2: Photomicrograph of biotite crystals of normal size (left) and a larger aggregate of biotite crystals (right) in a rock sample taken from Forsmark (Sweden). All dark green to black minerals in the images are biotite crystals. Image reproduced with permission from Drake et al. [32].

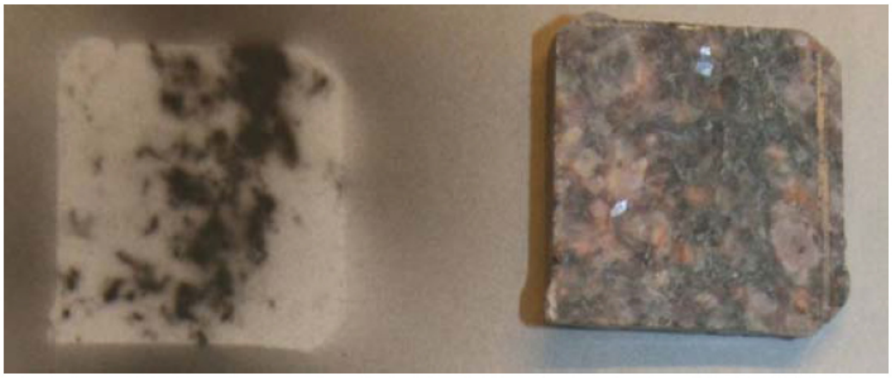

Figure 3: (left) Autoradiography analysis of core D7.1 from borehole KA3065A03 and (right) photography of the same core. The core was drilled and sampled after the finalisation of the Long Term Sorption Diffusion Experiment (LTDE-SD) at Äspö (Sweden). The basis of the slice is approximately 16 mm. The blackening on the autoradiograph represents radioactivity of primarily cesium (Cs-137). Figure reproduced with permission from Nilsson et al. [19].

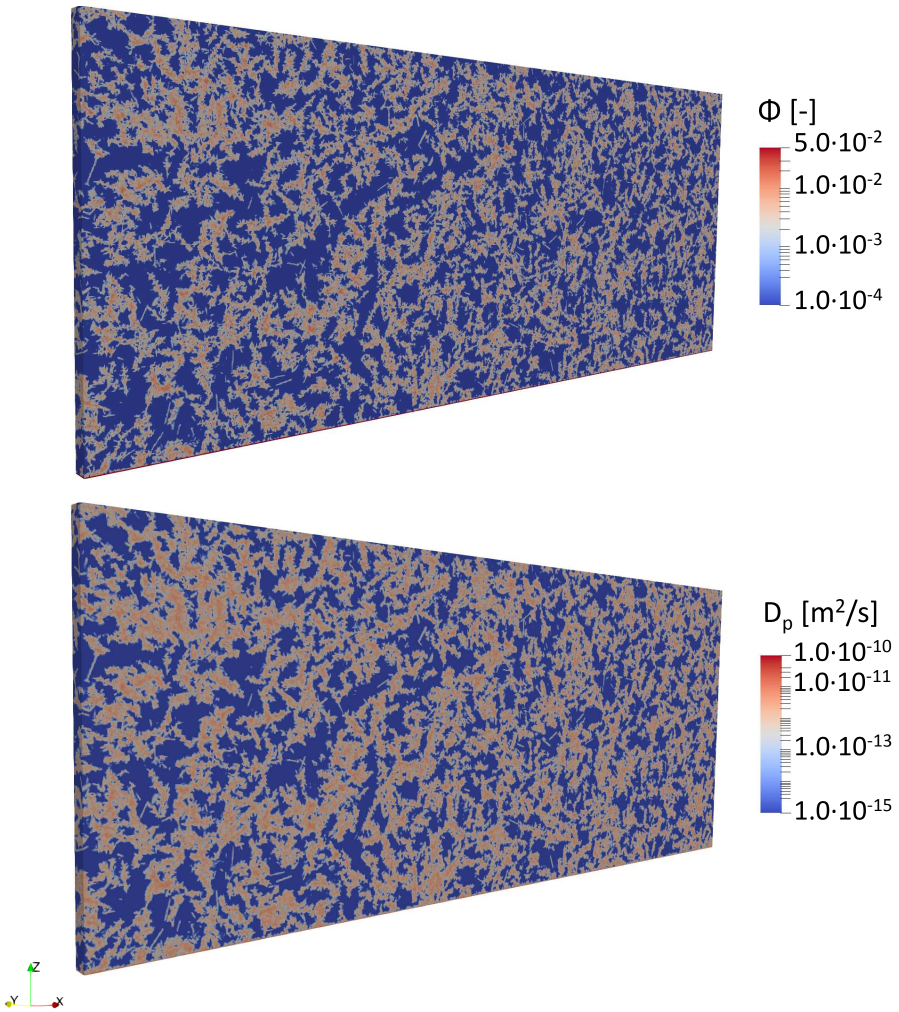

Figure 4: DFN-derived distribution of (top) porosity and (bottom) pore diffusivity as represented in the continuum model.

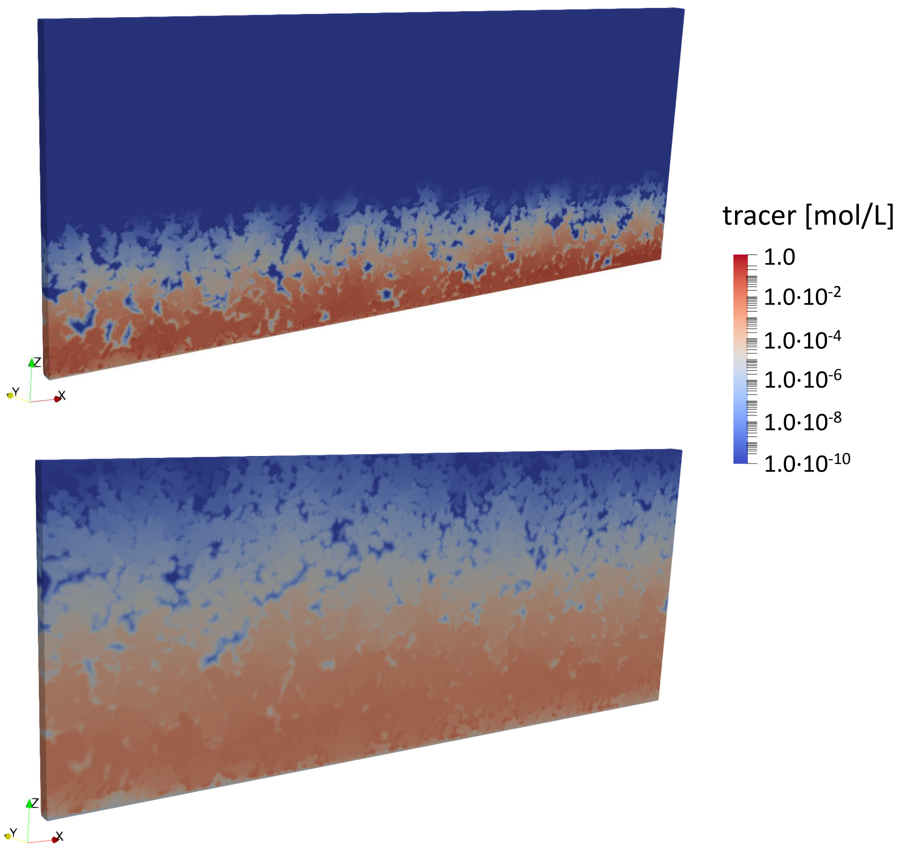

Figure 5: Snapshots of tracer concentration after (top) 1 yr and (bottom) 8 yr from the beginning of the injection.

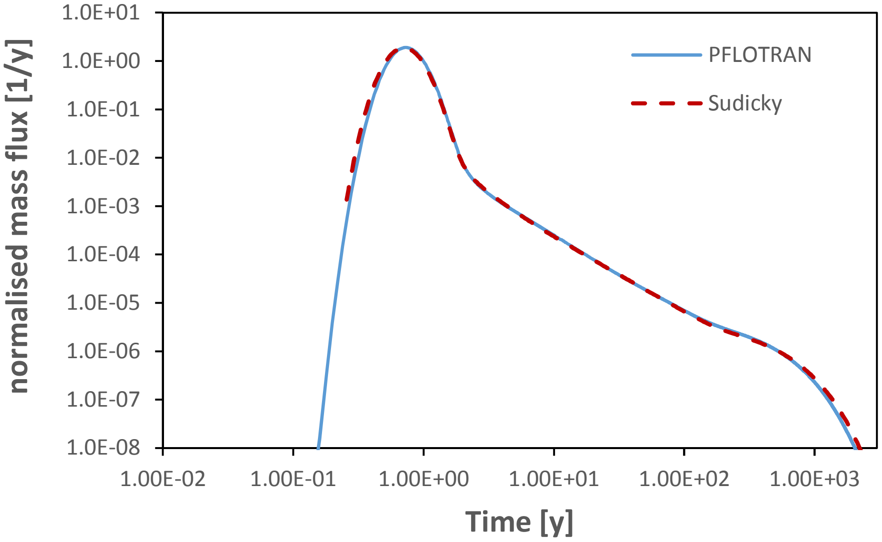

Figure 6: Breakthrough curve of a non-sorbing tracer computed with the “heterogeneous matrix model” (continuous line) and fit computed using equivalent parameters and Sudicky’s analytical solution [4] (dashed line).

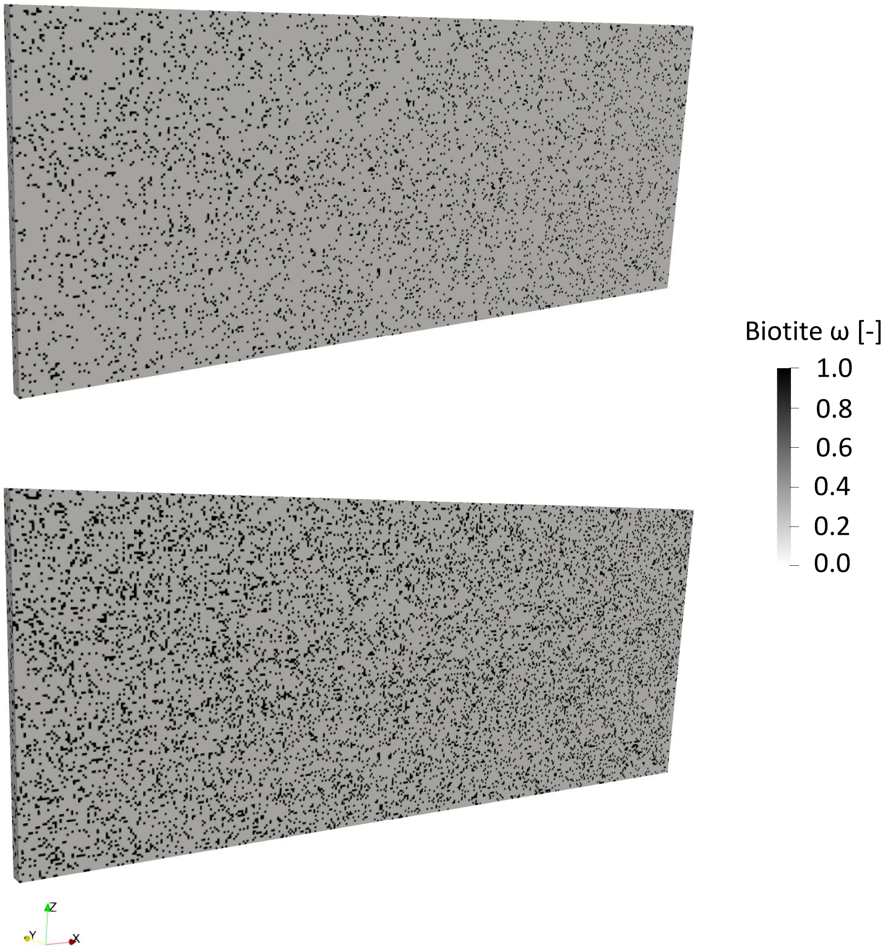

Figure 7: Biotite volume fraction for (top) MA, i.e. the model with 8% biotite and (bottom) MB, i.e. the model with 16% biotite.

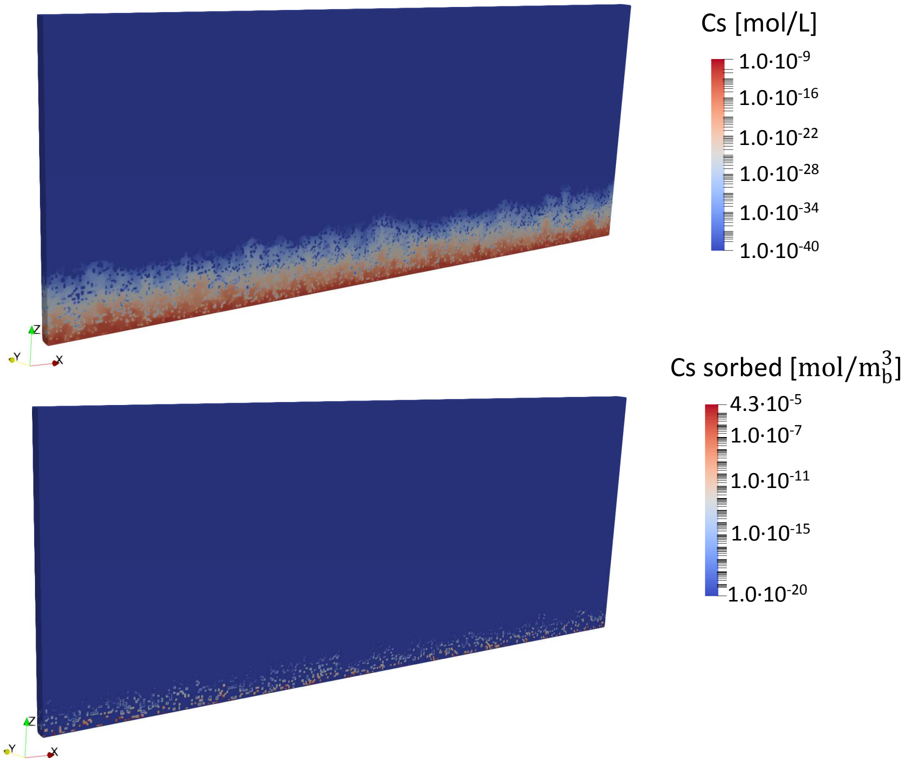

Figure 8: Snapshots of (top) cesium concentration and (bottom) cesium sorbed computed with MB after 30 yr from the beginning of the injection.

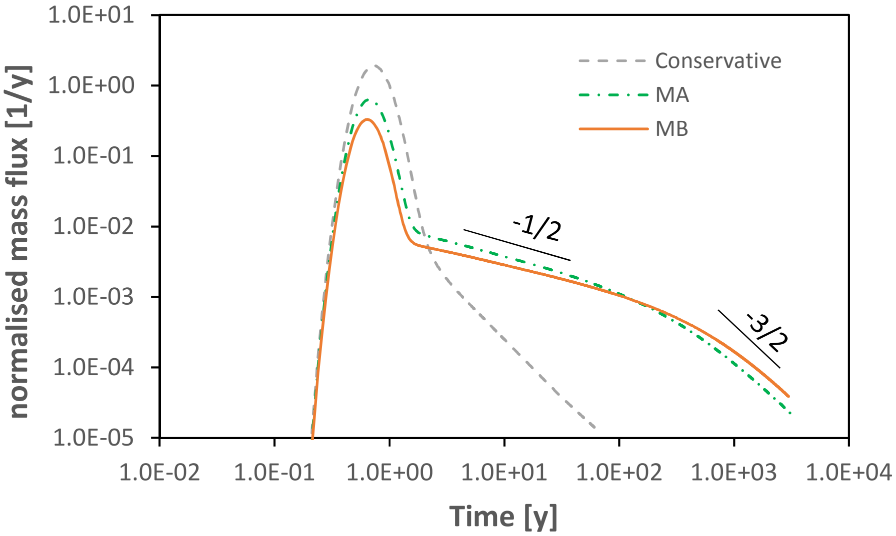

Figure 9: Cesium breakthrough curves computed with Model A (MA) and Model B (MB). The log-log slope of different parts of the tailings are also indicated.

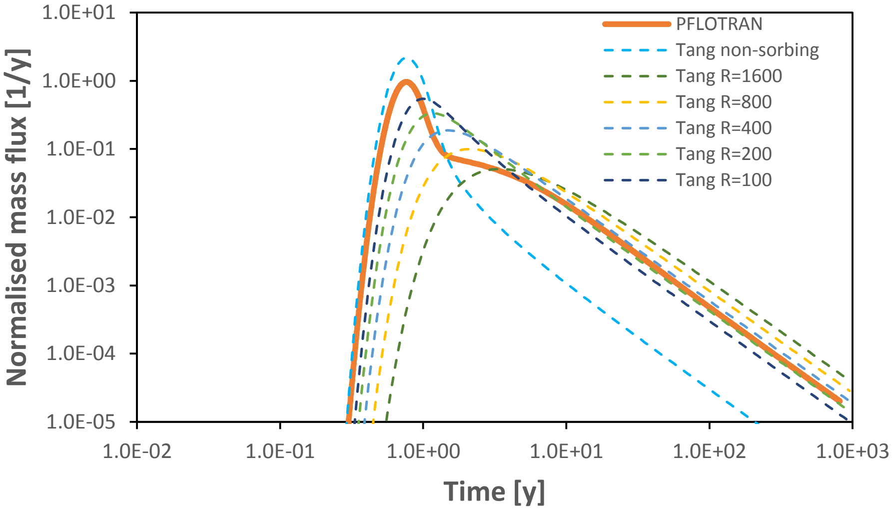

Figure 10: *Lab-scale* breakthrough curve (thick continuous orange line) computed with the 2D mineralogically heterogeneous model and with a bulk mineral volume fraction of the sorbing mineral $p = 0.16$. Homogeneous breakthrough curves computed using Tang's solution [3] and with different retardation values in the matrix are also shown.

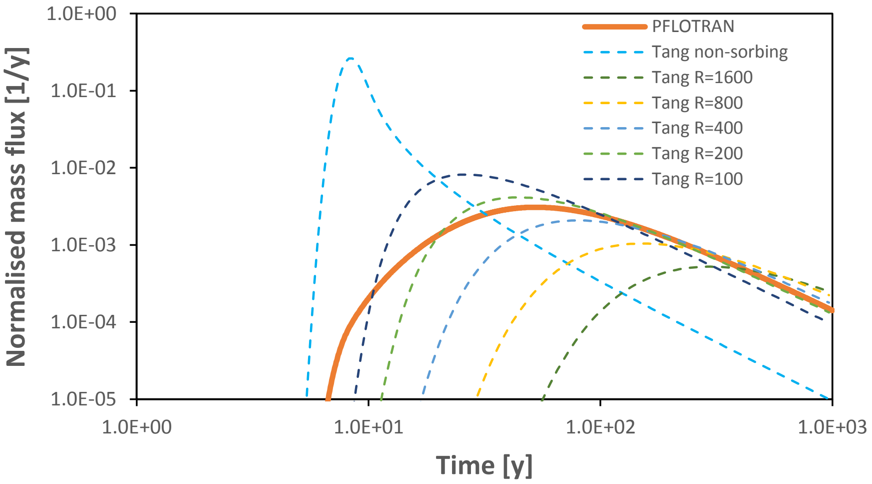

Figure 11: *Field-scale* breakthrough curve (thick continuous orange line) computed with the 2D mineralogically heterogeneous model and with $p = 0.16$. Homogeneous breakthrough curves computed using Tang's solution [3] and with different retardation values in the matrix are also shown.

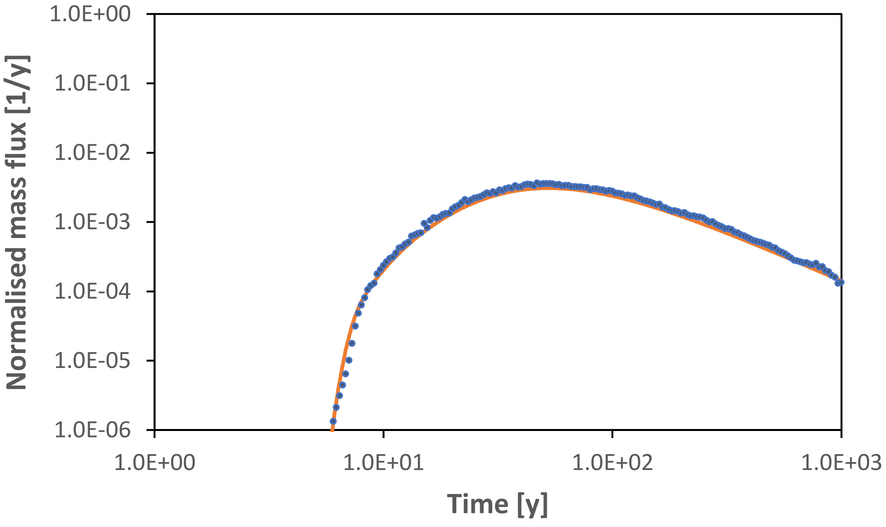

Figure 12: *Field-scale* breakthrough curve computed with (thick continuous orange line) PFLOTRAN and the 2D mineralogically heterogeneous model and with (blue dots) MARFA using the DS approach and 10 equally time-space segments.

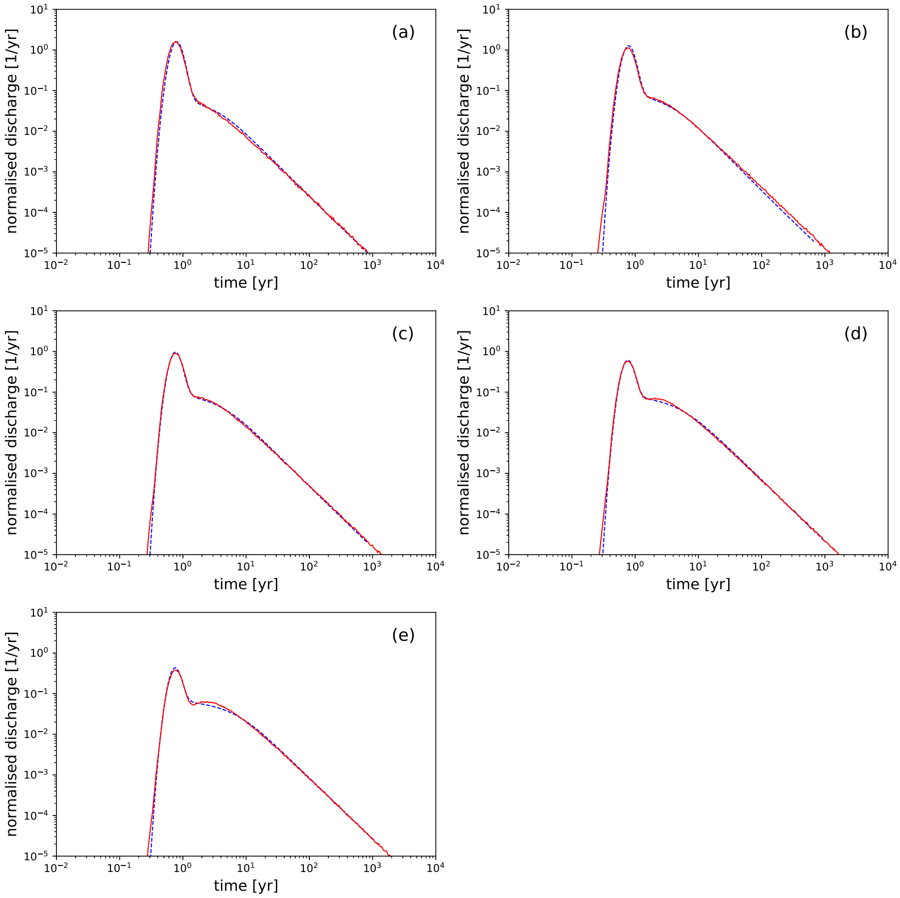

Figure 13: *Lab-scale* breakthrough curves computed with (dashed blue lines) PFLOTRAN and with (continuous red lines) MARFA using the TPPM and a single segment. Different sorbing mineral volume fractions are considered; namely (a) $p = 0.04$, (b) $p = 0.08$, (c) $p = 0.16$, (d) $p = 0.32$ and (e) $p = 0.5$.

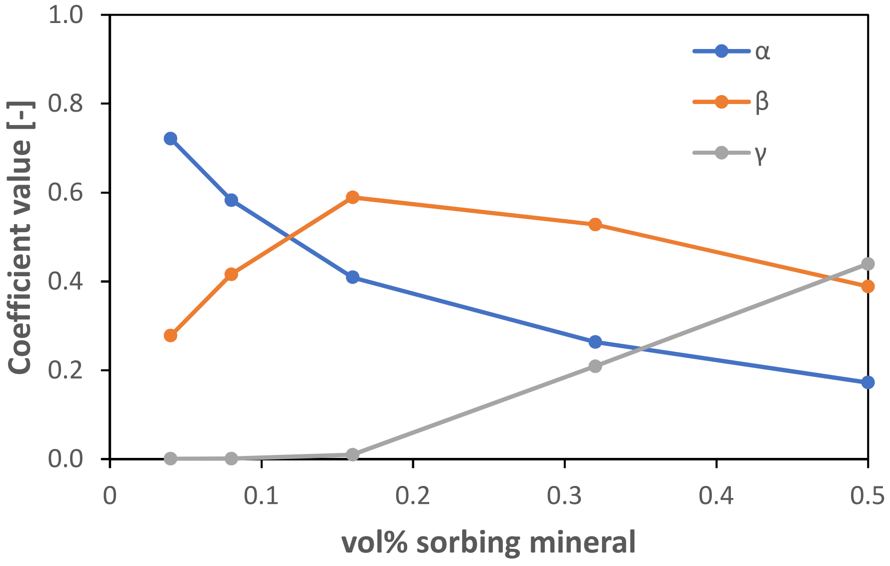

Figure 14: Coefficients of the TPPM estimated from the different *lab-scale* experiments (Figure 13).

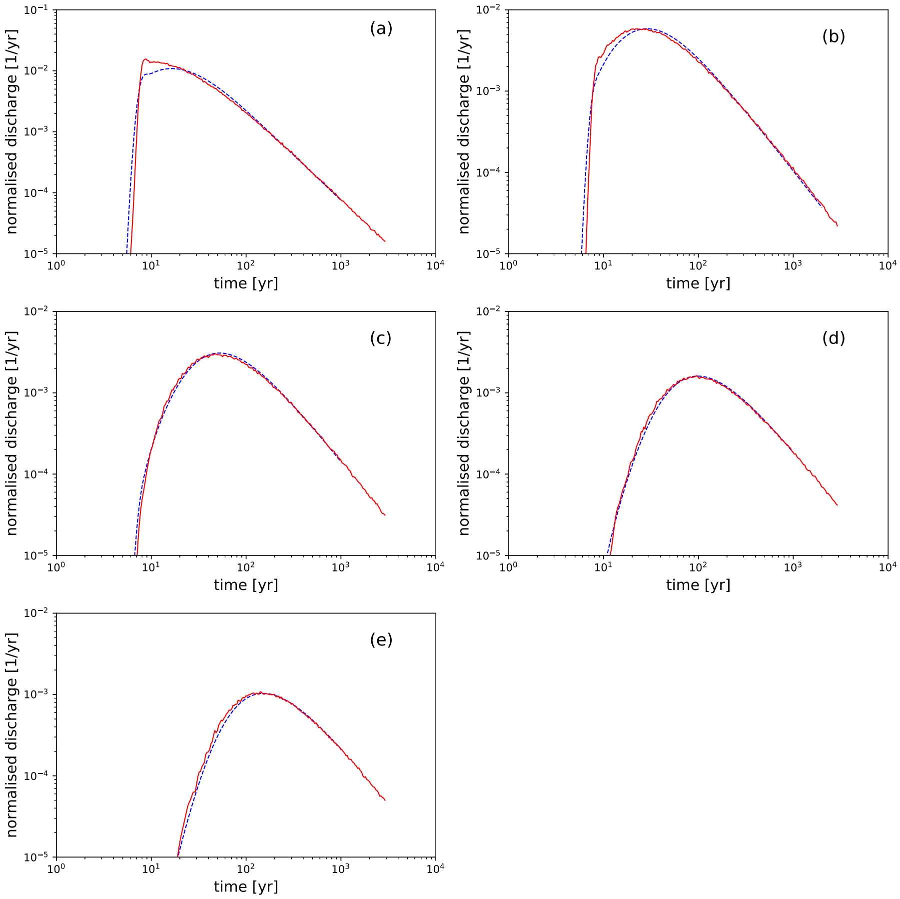

Figure 15: *Field-scale* breakthrough curves computed with (dashed blue lines) PFLOTRAN and with (continuous red lines) MARFA using the TPPM and ten equally spaced segments. Different sorbing mineral volume fractions are considered; namely (a) $p = 0.04$, (b) $p = 0.08$, (c) $p = 0.16$, (d) $p = 0.32$ and (e) $p = 0.5$. The coefficients of the TPPM used in the calculations are shown in Figure 14.

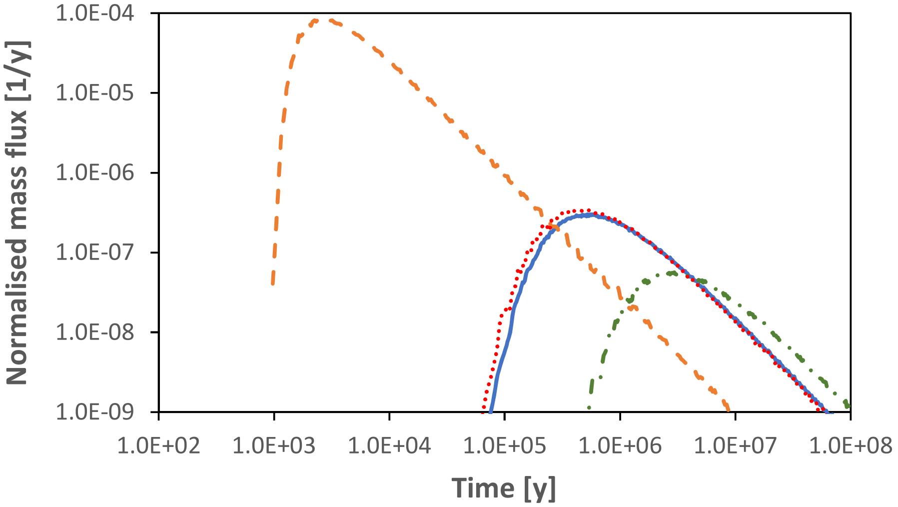

Figure 16: *Site-scale* models with contant transport properties. The heterogeneous breakthrough curve is computed with (continuous blue line) the TPPM and 1000 equally spaced segments (each segment of 0.25 m length) with $p = 0.16$. Homogeneous breakthrough curves computed with (orange dashed line) no sorption, (green dashed-dotted line) R=1,600 and (red dots) R=250 (i.e. $K_d = K_d^g \cdot p$) are also shown.

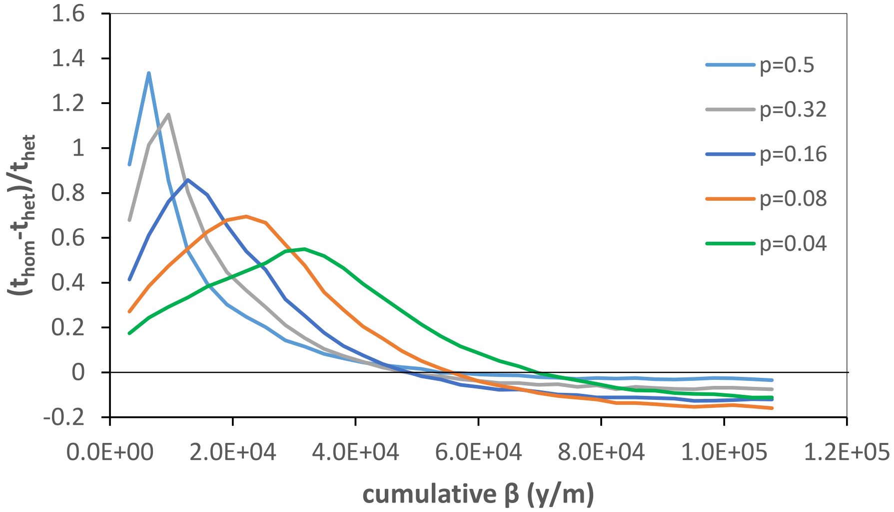

Figure 17: Relative difference between the first arrival time (1% of total injected mass) for the TPPM (t_{het}) and the equivalent homogeneous model (t_{hom}) for the five considered sorbing mineral volume fractions as a function of the cumulative transport resistance β.

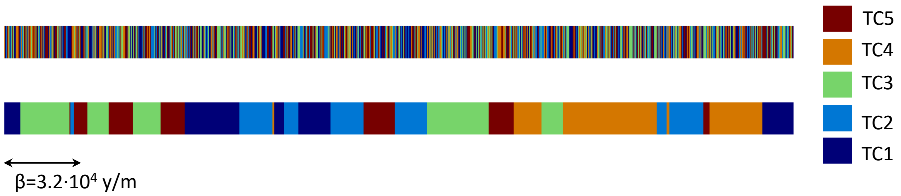

Figure 18: Distribution of the five transport classes for (top) the uncorrelated and (bottom) the correlated longitudinally heterogeneous model.

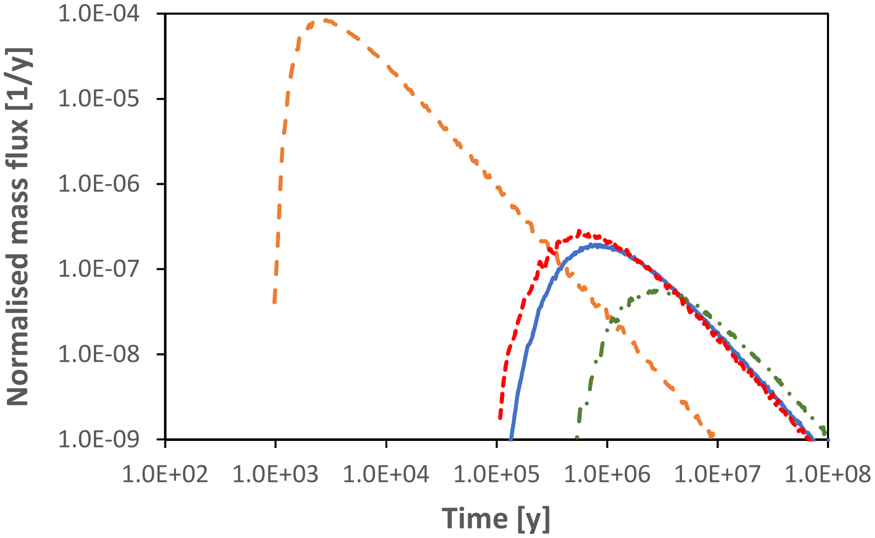

Figure 19: *Site-scale* models with different transport classes. The longitudinally heterogeneous breakthrough curve is computed with (continuous blue line) the TPPM and 1000 equally spaced segments (each segment of 0.25 m length) with the distribution of p shown in Figure 18 top. Homogeneous breakthrough curves computed with (orange dashed line) no sorption, (green dashed-dotted line) R=1,600 and (red dots) R=352 (i.e. $K_d = K_d^g \cdot < p >$) are also shown.

Appendix A. Implementation of the TPPM in MARFA

For each particle that is routed along a segment a random number is drawn, $R \sim U([0,1])$ and the conditional sampling is performed following the pseudocode listed below:

```
if $R \leq \alpha$ then
    $f_{ret} = f_{ret}^{ns}$
else if $R \leq \alpha + \beta$ then
    $f_{ret} = f_{ret}^{ms}$
else
    $f_{ret} = f_{ret}^{hs}$
end if
```

The correct implementation of the conditional sampling scheme has been verified by comparing the results of a MARFA transport calculation carried out along a single segment with the results obtained using an analytical solution based on Equations 6, 7 and 8 (results are not shown here for the sake of brevity).